Simulation of the interaction of high-energy C_{60} cluster ions with amorphous targets

E. Nardi* and Z. Zinamon
Department of Particle Physics, Weizmann Institute of Science, Rehovot 76100, Israel

T. A. Tombrello and N. M. Tanushev
Basic and Applied Physics, California Institute of Technology, Pasadena, California 91125
(Received 19 October 2001; published 11 July 2002)

Detailed simulations of the interaction of energetic C_{60} beams with amorphous targets are presented here. The spatial evolution of the cluster components is calculated accounting for multiple scattering and Coulomb explosion by means of Monte Carlo and molecular dynamics, respectively. The charge states of the individual cluster components (atoms, atomic ions, fragment cluster ions) as a function of penetration depth are also calculated in tandem with the above calculations by means of the Monte Carlo method. The relative importance of scattering versus Coulomb repulsion is studied as a function of the C_{60} cluster energy. The effect of the neighboring cluster constituents on the average charge state of the cluster atoms is calculated as a function of the depth of penetration for a C_{60} cluster of 40 MeV. The calculation accounts for the increase in ionization energy of the atom due to the other constituents. Relative track radii are calculated as a function of penetration depth and good agreement with the experimental results is obtained for the interaction of a 30 MeV carbon cluster with silicon. Track splitting observed well into the target as measured by Dunlop *et al.* in yttrium iron garnet is obtained in the simulations described here for the case of amorphous carbon, provided the Coulomb repulsion is screened by the four valence electrons. Collective energy deposition enhancement is calculated for the 720 MeV cluster. Here the cluster constituents are nearly fully ionized, thereby minimizing the ambiguity related to the value of the ionic charge in the calculation.

DOI: 10.1103/PhysRevA.66.013201 PACS number(s): 36.40.−c, 34.50.Bw, 34.70.+e, 34.50.−s

I. INTRODUCTION

The study of the interaction of energetic C_{60} beams with solid targets has been the subject of considerable experimental effort and has yielded substantial results of much interest. In particular, the work on the interaction of C_{60} beams of up to 40 MeV with metals [1], $Y_3Fe_{13}O_{12}$ (YIG) [2], and other insulators [3] has given rich data on the morphology of track formation as well as on damage. Other work dealing with the charge state, sputtering, and secondary emission due to the interaction of energetic carbon clusters with solids has also recently been published [4,5]. We also note the experimental observation that the charge state of the individual ions of the cluster exiting the target can be suppressed by up to 30% of their value relative to the corresponding ionic charge state of atomic beams [5]. In general, the bombardment of solids with energetic clusters provides a unique means of obtaining very high electronic energy deposition in this medium, essentially unattainable by other deposition processes; this topic is thus one of special interest. Another topic of particular interest is the study of the influence of the so-called vicinage effect, the effect of the electronic excitations produced by neighboring projectiles on the energy deposition of the cluster. The neighboring projectiles lead to interferences in the excitation of individual and collective modes, thereby influencing among other things the energy loss. The vicinage effect is of special interest here since C_{60} is a closely packed many-atom system where these phenomena can manifest themselves.

A basic prerequisite to understanding the processes involved in the interaction of C_{60} with solid targets is the knowledge of the spatial evolution of the cluster. This is particularly important for understanding track formation [6,2,3], enhanced energy loss [7], and secondary electron and ion emission [1]. Track formation, which is studied here, is a result of the damage inflicted on the target by the projectiles. It is mostly confined to cylindrical regions around the path of the projectiles and is seen clearly in electron micrographs where it is observed as tracks going through the irradiated material. In this connection, Ramos *et al.* [3] studied the spatial correlation of the cluster components as a function of the penetration depth from damage profiles and track length measurements. The work of Dunlop *et al.* [2] should also be mentioned within this context, especially with respect to the production of tails at the end of the track. In this study we calculate the spatial evolution of energetic C_{60} clusters due to both multiple scattering of the individual cluster components with the target atoms, and to the process of Coulomb explosion. Both processes were calculated simultaneously; the multiple scattering was calculated by means of the Monte Carlo method and the Coulomb explosion using molecular dynamics. Work similar to this was carried out by Tombrello *et al.* [6], who calculated the breakup of C_{60} in YIG, and also by Hartman *et al.* [8] for smaller clusters. Various aspects of the interaction of clusters with solid targets were also studied by Sigmund *et al.* [9]. The relative importance of Coulomb explosion versus multiple scattering as a function of cluster energy is stressed in our study, in which the calculations are

*Email address: fneran@wis.weizmann.ac.il

performed for an amorphous carbon target. The spatial correlation of the cluster components was studied as a function of penetration depth in order to predict formation of tracks in silicon and track splitting in amorphous carbon, using the reasoning presented in Ref. [6]. Special emphasis was put on the breakup of the cluster into smaller clumps at relatively large depths as observed by Dunlop *et al.* [2]. In this context the interparticle screening strongly influences the results.

The influence of the other cluster components on the ionic charge state of the cluster constituent was studied by calculating the change in the electronic binding energy of the latter. These calculations were carried out as a function of cluster penetration. Collective energy deposition enhancement was also investigated as a function of cluster kinetic energy and of penetration depth of the cluster into the target. The predictions of these calculations could be experimentally tested, since carbon is a material from which very thin targets can be fabricated.

In Sec. II we describe the basic model as well as the calculational procedures. The results are presented in Sec. III, where the following topics are addressed: cluster expansion, and the relative importance of Coulomb repulsion compared to scattering; track formation as studied on the basis of the spatial correlations between the cluster constituents as they penetrate the target; charge state of the cluster components as a function of the penetration depth and collective energy deposition enhancement for high-energy clusters. In each of these topics the physics of screening of the target valence electrons plays a prominent role. In Sec. IV we conclude.

II. THEORY AND CALCULATIONS

In order to investigate the physical phenomena outlined above, what is needed is to provide a computational method that determines how the trajectories of the individual atoms of the cluster evolve as they move deeper into the target. In the following a hybrid algorithm similar to the one given in Refs. [6] and [8] is described. The cluster constituents upon penetrating the target suffer multiple binary collisions with the target atoms, causing them to scatter and change direction. This multiple-collision scattering process is treated in more detail below. Between these collisions intracluster Coulomb repulsion forces act upon the cluster ions. There forces are responsible for the process termed Coulomb explosion, which refers to the expansion of the cluster due to the Coulomb forces only. The ions in the present problems are comoving and relatively close; thus several or many of the cluster constituents may be in the range of one another during the relatively long time of cluster penetration within the target. Therefore, a full molecular dynamics integration of the intracluster forces is required, which should be carried out in conjunction with the binary scattering. Some details of the molecular dynamics calculation are outlined below. The Coulomb interaction between the cluster components is governed by the effective charge of each of these components, which must be determined as a function of cluster penetration for each individual component. As will be shown below the charge state is also dependent on the positions of the neighboring cluster components. In the following we describe in more detail the computational methods involved in these three basic processes, starting with the determination of the effective charge state.

The charge-state evolution of the cluster constituents, the knowledge of which is imperative for the Coulomb explosion calculations, was calculated for each individual cluster component as a function of penetration depth. The calculations are based on a model developed by Bell [10] and were described by us for similar applications in Refs. [11] and [12]. These calculations involve the capture and loss of electrons by the carbon projectiles. Loss of the projectile electrons is due to ionization resulting from the Coulomb interaction of the bound projectile electrons with the target atoms, using the binary encounter approximation (BEA) [13]. Using this model some adjustment is needed in determining the value of the effective target atom charge as prescribed by Bell. The electron capture cross section is calculated in two stages. In the first stage the cross section for the liberation of a target electron by the charged ion is calculated. Following this it is determined whether the liberated target electron is captured by the projectile, depending on whether the potential energy of binding is greater than the kinetic energy of the electron in the projectile rest system. It is important to add that the very short early stage of loss of molecular stability is neglected, and it is assumed that the cluster initially is composed of neutral carbon atoms at their original positions in the cluster. Thus it should be stressed that the model here treats the cluster constituents as individual atoms, disregarding the possible effect of collective cluster states.

The above method for calculating the charge states of the individual carbon cluster components makes possible the calculation of the influence of the neighboring cluster components on the charge state of the given carbon ion. Following Hartman *et al.* [8] the change in the ionization potential of a given bound electronic level ΔI_i is

$$\Delta I_i = \sum_{j(\neq i)} q_j \left(\frac{e^{-r_{ij}/a}}{r_{ij}} \right), \tag{1}$$

where r_{ij} is the distance between the ith atomic ion and the given ion and a is the screening length of the target electron gas to be discussed below. By thus increasing the binding energy of the projectile electron and in accordance with the BEA model employed here, the ionization cross section of the bound projectile electrons becomes smaller compared than in single-atom case. Basbas *et al.* [14] previously calculated ΔI_i in low-energy particle encounters and used this for calculating corrected K-shell ionization cross sections. These authors based their calculations on first-order perturbation theory. The effect of the neighboring charged particles within the cluster on the electron recombination cross section was not accounted for here. This effect will be accounted for in future calculations.

The scattering of each of the cluster components by the target atoms is treated independently. The simulations were carried out using the binary collision model, devised for

amorphous targets, of Moller *et al.* [15]. The ion-atom potential used in these calculations is due to Lindhard *et al.* [16] and is given by

$$V_{\mathrm{IA}}(r)=(Z_1Z_2/r)\,\phi(r/a_{\mathrm{TF}}),$$

where r is the projectile-target distance and

$$a_{\mathrm{TF}}=0.8853a_B(Z_1^{2/3}+Z_2^{2/3})^{1/2},$$

with Z_1 and Z_2 the projectile and target atomic charge numbers and $\phi(r/a)$ a dimensionless universal Thomas-Fermi function. Based on this potential a differential scattering cross section was also derived by Lindhard *et al.* [16] and is used here. It is assumed that each scattering center is effective within a spherical volume of radius equal to half the average distance between neighboring atoms, thus determining the collision probability per path length. The distance between successive multiple collisions is randomized and chosen statistically by means of the Monte Carlo method. The center-of-mass scattering angle is expressed in the reduced unit z, which also contains the particle center-of-mass energy. Lindhard *et al.* [16] have shown that the reduced scattering cross section J for the potential V_{IA} given above can be written as

$$dJ/dz=f(z)/z^2, \tag{2}$$

where $f(z)$ is a function derived by Meyer [17].

At each collision the polar angle θ is obtained by sampling the function J in Eq. (2) by means of the Monte Carlo method. The isotropically distributed azimuthal scattering angle is chosen randomly. The new projectile directions are then transformed to the laboratory coordinates. The details of the simulation are given by Moller *et al.* [15] as well as by Zajfman *et al.* [18] who implemented this procedure.

The forces driving the Coulomb explosion are derived from the screened two-body Coulomb potential,

$$V_c=(q_iq_j/r)\exp(-r\sqrt{2}/a), \tag{3}$$

where q_i and q_j are the charges of the ions i and j, r is the distance between them, and a is the screening length, given by $a=v_p/\omega_p$, with v_p the projectile velocity and ω_p the plasma frequency of the valence-electron gas. The number of screening electrons was assumed equal to 4, equal to the number of carbon valence electrons. Vager and Gemmell [19], based on the plasmon energy needed to fit their experimental data, obtained a value of 4.5 electrons per carbon atom, in good agreement with the number of the plasma or screening electrons assumed here. The screening length was divided by $\sqrt{2}$ in order to account for screening between two electron clouds [20].

A more accurate account of the intracluster interaction can be obtained following Vager and Gemmell [19], who also included the wake forces generated by the cluster components in the electron gas in addition to the Coulomb repulsion potential. It could be argued that in large clusters the wake forces become incoherent as the cluster penetrates into the medium.

In the molecular dynamics simulation, the equations of motion of the system, consisting here of the 60 carbon ions, are integrated, using forces calculated as the sum over pairwise interactions governed by the two-body screened Coulomb potential, as given in Eq. (2). Physically there must also be a hard-core potential, as was included in Refs. [6] and [8]. In the present calculations, this potential can be neglected due to the Coulomb repulsion between the ions. The equations of motion are solved in a series of time steps Δt, at each of which the force on each ion is calculated due to the interaction with the other ions of the system.

Having found the total force $\boldsymbol{F}$ on each particle, we integrate the equations of motion for each of the particles between times $n\Delta t$ and $(n+1)\Delta t$ using the leapfrog algorithm [21]:

$$v^{n+1/2}=v^{n-1/2}+(\Delta t/m)\boldsymbol{F}^n,$$

$$r^{n+1}=r^n+\Delta t v^{n+1/2}.$$

The velocity at step n is calculated as

$$v^n=\tfrac{1}{2}(v^{n+1/2}+v^{n-1/2}).$$

The calculation proceeds until the position of the particles given by the coordinates r reaches a given depth.

The calculation involves two basic time steps. The smaller of the two, Δt_z, is applied in the charge-state determination. This time step is chosen such that the probability of a change of charge state within the path determined by Δt_z is less than 25%. The larger time step Δt_{sc} gives the path length in the molecular dynamics and multiple-scattering computational step. The molecular dynamics calculation [21] is first carried out within this time step. At the end of this time step the particle directions are corrected for the multiple scattering. These new directions are then used as the initial directions of motion in the following molecular dynamics time step. Δt_{sc} is determined such that the probability of scattering within the path length defined by Δt_{sc} is not more than 20%. The multiple-scattering procedure was tested by calculating with it the radial transverse distribution of carbon atoms at 0.667 MeV transmitted through an amorphous 200-nm-thick carbon target. The results of these calculations were compared to those obtained by TRIM [22] for the same problem, and very good agreement between the two methods was obtained.

The molecular dynamics, Coulomb explosion procedure of the present paper was tested by calculating the average cluster radius for a 40 MeV C_{60} cluster with charge state of 2, and no screening between cluster components. The results of this calculation gave an average radius of 2.07 nm at a depth of penetration of 100 nm. This compares favorably with the calculation of Dunlop *et al.* [2], who approximated the C_{60} cluster by a homogeneously charged spherical sphere, obtaining a radius of 2 nm at the depth of 100 nm.

The energy loss of the C_{60} cluster which brings into account coherent stopping effects (vicinage effects) of the cluster components was calculated according to Arista [7], whose formulation is within the linear response approximation. Such calculations were performed in Ref. [12] for an electron

gas that represented the conduction electrons of a solid aluminum target. The details of these calculations are given in this reference, where we use the Lindhard dielectric function [23] rather than a more realistic one. In this connection, Abril *et al.* [24] made detailed comparisons of stopping powers in different forms of allotropic carbon, treating the four valence electrons both as a Lindhard gas and by the more elaborate Mermin [25] dielectric function, which is based on optical data. These authors concluded that above a carbon projectile kinetic energy of 2.5 MeV the simpler Lindhard function gives similar results to the Mermin dielectric function. Thus, for the total cluster energies of 144 and 720 MeV, for which the kinetic energies of the carbon projectiles are 2.4 and 12 MeV, it was assumed here that the Lindhard dielectric function gives an adequate description of the medium. We also confirmed that the stopping calculated using the Lindhard function at these two energies agrees satisfactorily with experiment.

The stopping formula according to Arista [7] is given in Eq. (4), where $\epsilon(\vec{k},\vec{k}\cdot\vec{v})$ is the dielectric function of the stopping medium, while q_i and q_j are the ionic charges. Problems arising with the definition of q_i and q_j in the context of collective stopping will be discussed below:

$$\frac{dW}{dt} = -\sum_j \vec{v}\cdot\vec{F}_j = \frac{e^2}{2\pi^2}\,\mathrm{Im}\left(\frac{-1}{\epsilon(\vec{k},\vec{k}\cdot\vec{v})}\right) \times\left(\sum_i q_i^2 + \sum_{i\neq j} q_i q_j \cos(\vec{k}\cdot\vec{r}_{ij})\right). \tag{4}$$

The first term in the second large parentheses gives the energy loss of the individual independent charges while the second term gives the interference effects due to charges in correlated motion.

III. RESULTS

A. Cluster expansion

Calculations were carried out for three different cluster kinetic energies 40, 144, and 720 MeV. The target was amorphous carbon at a density of 2.3 g/cm^3. In Fig. 1 is plotted the average cluster radius R_{av} as a function of penetration depth for a 40 MeV C_{60} cluster. The combined effects of Coulomb repulsion assuming four screening electrons plus multiple scattering are plotted in Fig. 1. Also plotted in Fig. 1 is the average cluster radius assuming multiple scattering only. Ten different random sequences were run in each of the cases for the multiple-scattering procedure but only the minimum and maximum radial expansions were plotted. The same random sequences were used for both cases. The results indicate that the multiple-scattering process is the dominant one at this energy, although at penetration depths less than 100 nm the effect of the Coulomb explosion is not negligible. The number of screening electrons is assumed equal to 4, and the screening length is set equal to 0.85 Å. The statistical spread of the average radius of the disintegrating cluster can be inferred from the results of these calculations. At a depth of 100 nm the total width of the distribution

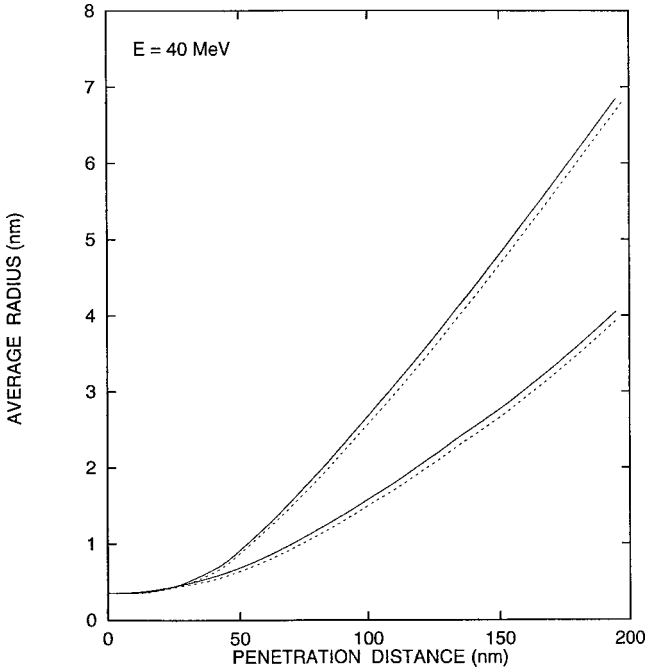

FIG. 1. Average cluster radius as a function of penetration depth for a 40 MeV C_{60} cluster. Dashes indicate multiple scattering only and the full line the combined effect of multiple scattering and Coulomb explosion. Of the ten simulations, only the two with the minimum and maximum values of the radii are plotted for both cases.

divided by the average radius is of the order of 50%. These results could be related to the statistical spread in the track diameter as observed experimentally by Ramos *et al.* [3] and by Dunlop *et al.* [2]. Both Ramos *et al.* [3] and Dunlop *et al.* [2] also estimated the relative contributions of scattering and Coulomb repulsion for C_{60} in the same energy range. In both of the above quoted works scatter was approximated using the TRIM code while the Coulomb repulsion was calculated using simplifying assumptions. These authors also found that the lateral spread due to multiple scattering significantly exceeds that of the Coulomb interaction.

In Fig. 2 we plot R_{av} as a function of penetration depth for a cluster energy of 144 MeV. Ten different random sequences were calculated assuming only multiple scattering. Again only the simulations giving the maximum and minimum expansions were plotted. There are approximately equal contributions to the expansion from multiple scattering and from Coulomb repulsion with four screening electrons. This is also seen in Fig. 2, which is based on ten different sequences that include multiple scattering as well as the above mentioned Coulomb term. Again, only the maximum and minimum radial expansions are plotted here. Finally, the average radii as a function of penetration distance are also calculated for the case of multiple scattering together with Coulomb repulsion assuming one screening electron. In the latter case Coulomb repulsion is the dominant process. We note here that on the basis of Fig. 2 scattering enlarges the C_{60} sphere by about a factor of 3 at a penetration depth of 150 nm. This result does not agree with the recent work of Wang *et al.*

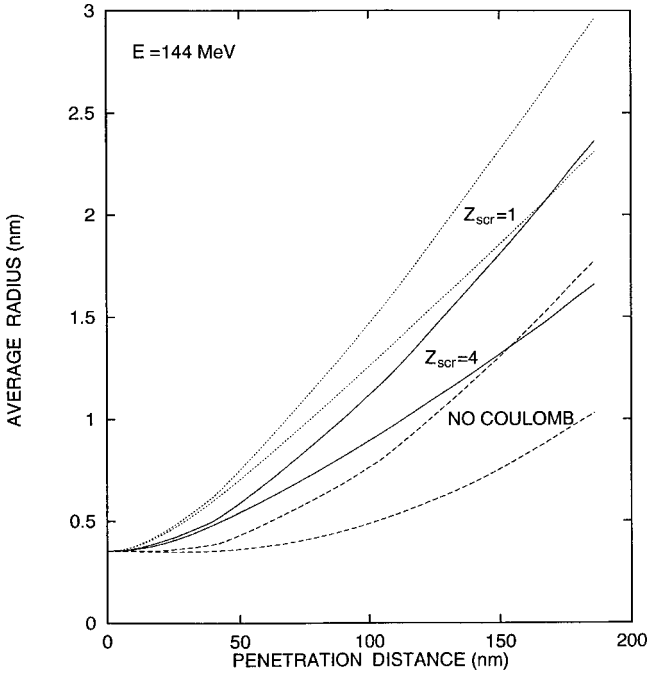

FIG. 2. Average cluster radius for a C_{60} 144 MeV projectile as a function of penetration depth. Dashes indicate multiple scattering only; full curve, multiple scattering with Coulomb explosion screening by four electrons ($Z_{scr}=4$); and dots, multiple scattering plus Coulomb explosion assuming one screening electron ($Z_{scr}=1$). Of the ten simulations computed for each of the three cases, only the minimum and maximum values of the radii are shown.

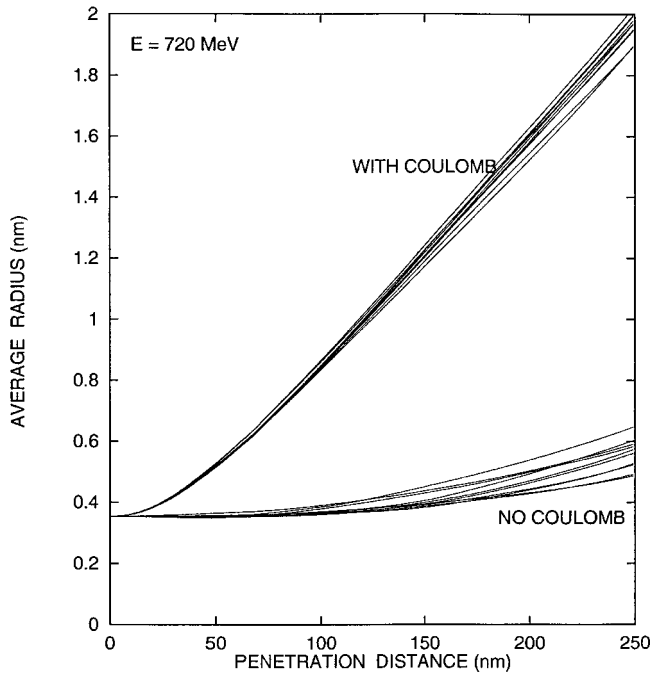

FIG. 3. Average cluster radius as a function of penetration depth for a 720 MeV C_{60} projectile, including multiple scattering only and with the combined effects of Coulomb explosion and multiple scattering. All ten simulations are plotted here for both of the cases.

[26], who disregard multiple scattering for energies close to the 144 MeV of our calculation, the results of which are presented in Fig. 2.

Finally, in Fig. 3, where R_{av} is plotted for a cluster with a total energy of 720 MeV, Coulomb repulsion between the cluster constituents, assuming once more four screening electrons, is by far the dominant process. Here all ten simulations are plotted. The penetration distance is taken to much larger values. Scattering decreases with increasing energy; thus the lateral spread of the C_{60} constituents decrease with increasing energy while the importance of the Coulomb term increases. It should also be noted that the screening length a increases with increasing energy. Therefore as the energy increases the screening of the Coulomb interaction becomes less effective: $a=0.85$ Å at 40 MeV, 1.6 Å at 144 MeV, and 3.6 Å at 720 MeV.

In summary, at the cluster energy of 40 MeV the dominant mechanism determining cluster expansion is the scattering of the individual cluster components on the target atoms. At the highest cluster energy treated here, 720 MeV, the dominant mechanism is the Coulomb repulsion between the cluster ions, also termed the Coulomb explosion. At the intermediate energy of 144 MeV both of the above mentioned processes are approximately of equal importance in determining the cluster expansion. These conclusions are based on the assumption discussed above that the intracluster Coulomb repulsion between the cluster ions is screened by four of the six carbon target electrons. The assumption that fewer target electrons screen the intracluster Coulomb repulsion would result in a more important role of the Coulomb explosion in the cluster expansion, as shown above.

B. Charge-state suppression

Equation (1), due to Hartman *et al.* [8], describes the additional ionization potential experienced by the electron bound to a given cluster ion due to the sum of the charged neighboring ions. According to the BEA used here for calculating the ionization cross section, the addition of ΔI_i in Eq. (1) to the binding energy causes a decrease in the ionization cross section. As noted above, the effects of the neighboring ions on recombination were not accounted for in the present calculations. In Fig. 4 is plotted the average cluster charge state as a function of penetration depth with and without the effects of the neighboring cluster ions as described by Eq. (1). The target is amorphous carbon and the cluster energy 40 MeV. The effect of the charge suppression, which decreases with increasing penetration, due to the gradual expansion of the cluster as seen in Fig. 4, is observed to persist up to about 450 Å into the target. Beyond 450 Å, the cluster components are too far removed to induce an observable increase in the ionization cross section. The magnitude of the charge suppression calculated up to about 150 Å into the target is about 20%. We note here that Hartman *et al.* [8] presented a phenomenological model for charge suppression that is based on the enhancement of electron capture due to the additional ionization potential. The inclusion of such an effect in our calculations would enhance the charge suppression effect, which attains values of up to 30% in smaller carbon clusters [5].

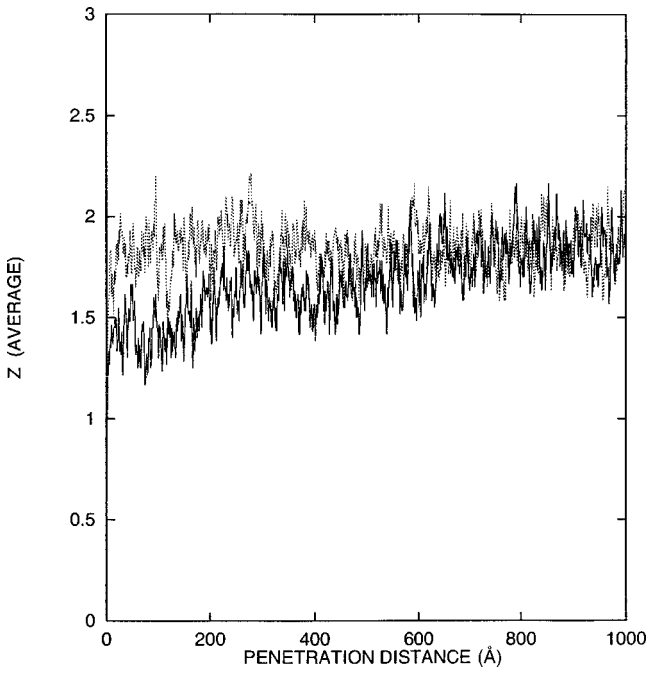

FIG. 4. Average charge state as a function of penetration depth for C_{60} at 40 MeV incident on amorphous carbon. Full curve includes the effect of neighboring cluster constituents on the ionization cross section. Points indicate the charge state with no effect due to neighboring ions.

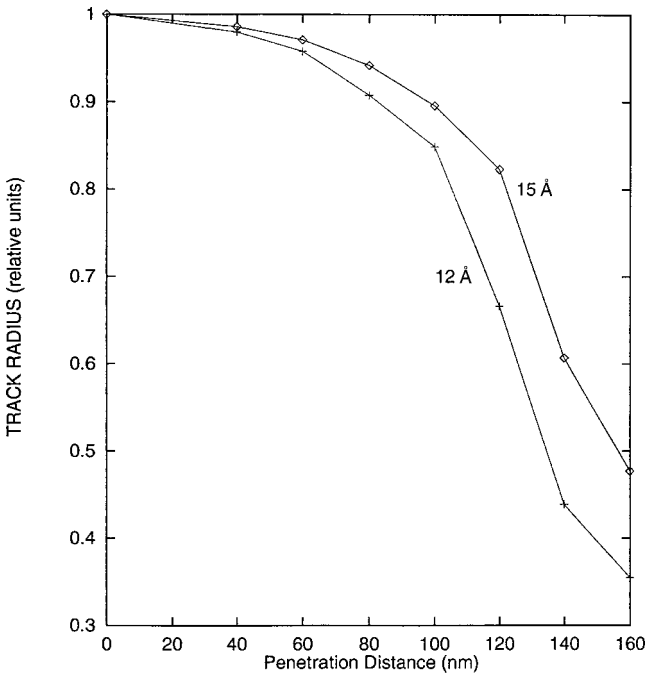

FIG. 5. Predicted relative track radius as a function of penetration depth for the interaction of a 30 MeV C_{60} cluster with an amorphous Si target. 12 Å and 15 Å are two different criteria for the overlap of δ electron clouds.

C. Track formation

The morphology of tracks in yttrium iron garnet was recently measured for C_{60} projectiles up to an energy of 40 MeV [2] as well as for crystalline silicon for C_{60} at 30 MeV [27,28]. These studies presented detailed experimental data on latent track radius R_t, total track length L_t, and the length over which the track radius remains constant, L_c. Beyond L_c it was observed that for YIG the observed tracks tail away to a point but in some cases two or three tails are produced. In the calculations presented here we have attempted to simulate the basic track behavior for crystalline silicon, in which the track is essentially cylindrical in shape up to a value of $L_c = 80$ nm, according to Ref. [26] and to about 50 nm according to Ref. [27]. However, the target in the calculation was amorphous silicon. We also study multitrack production as observed in YIG, simulating this by the interaction of 40 MeV C_{60} with an amorphous carbon target and not YIG.

Track production and splitting are determined here following the method of Tombrello *et al.* [6], based on the following assumptions, derived from experimental study of track production in YIG with different cluster sizes and at various incident kinetic energies [2]. The first relation deals with the connection between the track radius R_t and the deposited energy within the track volume:

$$\overline{e} = 0.178 \ \text{eV/Å}^3 = (dE/dx)/(\pi R_t^2). \tag{5}$$

Although this relation was obtained for YIG we use its basic form, which states that $R_t \sim (dE/dx)^{1/2}$ for the amorphous Si target. A second assumption involves determining the number of particles ''acting together'' to form the track, thus enabling the calculation of dE/dx as used in Eq. (5). This occurs when the δ electron clouds of adjoining particles coincide; thus the distance between these ions must be less than 10–15 nm. Thus R_t should decreases with increasing penetration distance since the number of ions ''acting together'' decreases with cluster expansion.

The constant in Eq. (5) is known for YIG, but has not been obtained for amorphous Si targets. We avoid this difficulty by calculating relative values of R_t as follows. At the projectile energies considered here for track analysis, the energy loss for a group of ions ''acting together'' is simply proportional to the number of ions in the group (no collective energy loss enhancement discussed in Sec. III D below). The energy loss along the track down to the point where it disappears is neglected, so that the dE/dx per ion is close to constant. Under these conditions the track radius according to Eq. (5) is proportional to the square root of the number of ions ''acting together.'' We assume that the initial radius of the track is determined by the 60 ions in the C_{60} cluster and this is defined to be the unit R_t. The relative radius at each point along the track is thus determined by the number of ions ''acting together'' at that point.

Using the above assumptions and calculating the interaction and breakup of a 30 MeV C_{60} cluster in an amorphous Si target, the relative value of R_t is determined and plotted in Fig. 5 as a function of penetration depth into the target. Two different assumptions regarding the criterion for overlapping δ electron clouds were used. R_t in Fig. 5 is observed to remain relatively constant up to between 50 and 80 nm and from here gradually decreases, in basic agreement with experiment. As is to be expected R_t is larger for the 15 Å

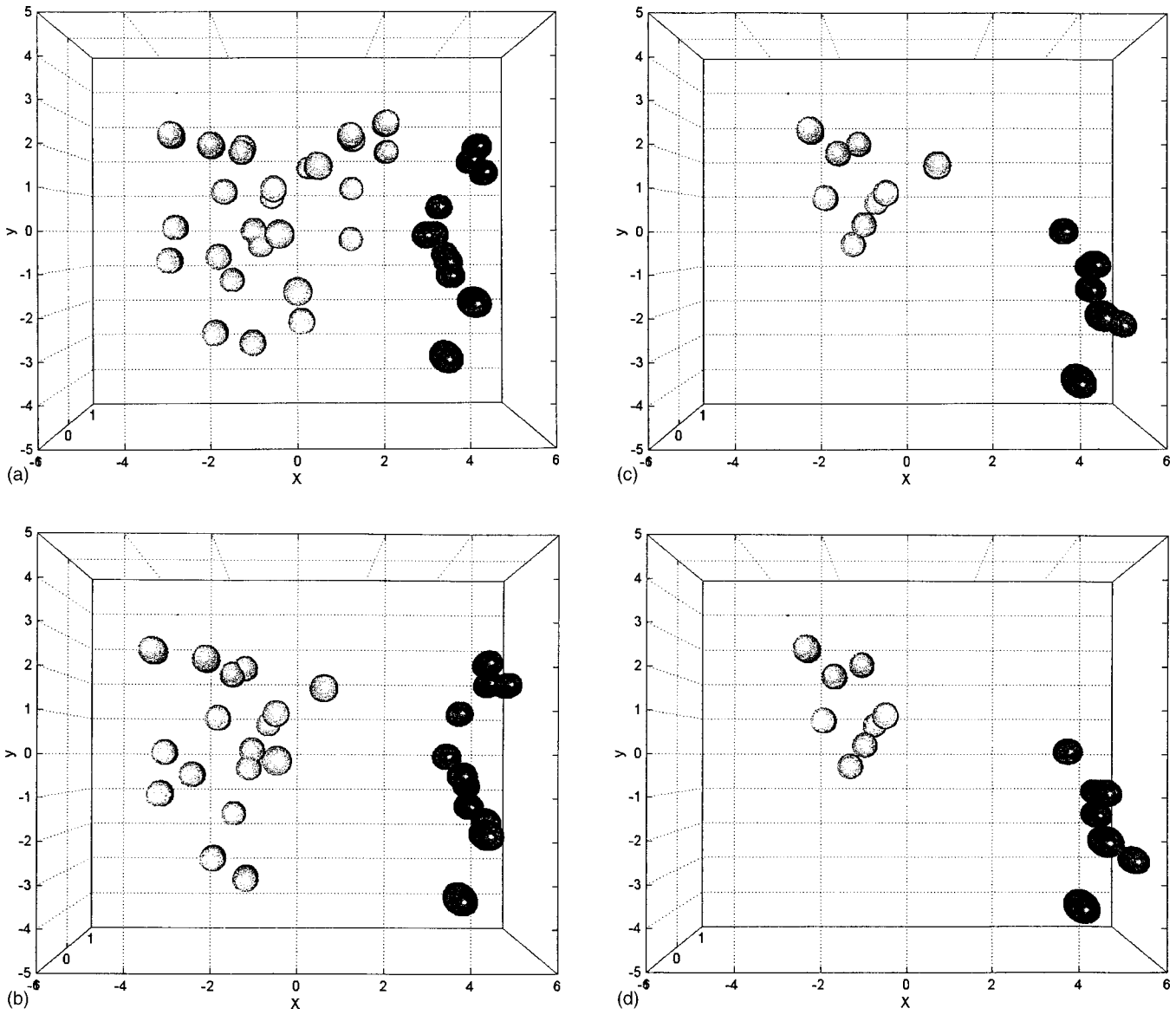

FIG. 6. Simulation of particle splitting for a 40 MeV C_{60} cluster on amorphous carbon. The minimum distance between clumps is denoted by $d_{\min}$ and the distance between the centers by d_{cnt}, both in nm. The two clumps at the penetration depth of (a) 180 nm, $d_{\min}=2.0$, $d_{\mathrm{cnt}}=4.6$; (b) 190 nm with $d_{\min}=3.6$, $d_{\mathrm{cnt}}=6.2$; (c) 195 nm with $d_{\min}=3.7$, $d_{\mathrm{cnt}}=6.4$; and (d) 200 nm, with $d_{\min}=4.8$ and $d_{\mathrm{cnt}}=6.8$.

criterion than for 12 Å. In order to be able to simulate track splitting, which involves the formation of tracks produced by a small number of particles, a criterion for the minimum number of particles able to form a track must be established. By examining the minimum radii of visible tracks and by the use of Eq. (4), Tombrello *et al.* [6] concluded that in YIG at least six carbon atoms ''acting together'' as defined above can produce a visible track. In the following we define aggregates of carbon projectiles capable of producing tracks as clumps. As above we apply this criterion to the case of the C_{60} cluster incident on amorphous carbon.

The interaction of a 40 MeV C_{60} cluster with amorphous carbon was simulated as described above. The simulation included multiple scattering and Coulomb repulsion with four screening electrons. A total of 25 simulations was run, the purpose of which was to obtain track splitting, which occurs toward the end of the track range. Particles were assumed to be in the same clump provided the distance between them was less than 15 Å; clumps were considered separated on condition that the minimum distance between them was 19 Å. Track splitting is defined for those events in which the separated clumps persist for 20 nm, with at least six of the clump constituents not leaving the clump. Track splitting is observed in Fig. 6, where at a depth of 180 nm the nearest the clumps get to each other is 19.9 Å and the distance between the clump centers is 46 Å. With increasing penetration depth the clumps are clearly seen to separate, where at the depth of 200 nm the nearest the clumps get is 47.8 Å while the distance between the clump centers is 68 Å. The number of particles in the clumps is observed to decrease with increasing penetration. Results similar to those of Fig. 6 were obtained in two other simulations, while basi-

cally no splitting at all was observed assuming screening by one electron. The simulation results for track splitting qualitatively confirm the experimental track splitting in YIG, in which this phenomenon occurred not too often.

D. Energy loss enhancement

The calculation of the cluster stopping including collective effects according to Eq. (3) involves ambiguity in connection with the definition of the ionic charge appearing in Eq. (3). This was pointed out by Jensen and Sigmund [29]. The effective projectile charge responsible for stopping depends on the impact parameter (IP). At small IP it is the nuclear charge while at large IP it is the ion charge. Coherent or collective stopping stems from large IP while incoherent or the stopping of the individual components involves both near and distant collisions [29]. Thus there exists an ambiguity in the value of q when calculating the stopping ratio R defined as the ratio of the total cluster stopping including the collective effects of the neighboring ions to the stopping of the sum of the individual cluster components. This problem can be alleviated by confining the calculations to systems that are nearly completely ionized.

The calculations were therefore carried out for the 720 MeV C_{60} cluster, where for penetration distances larger than 40 nm the ionic charge state reaches the value of 5 [see Fig. 7(a)]. Comparing this to the nuclear charge of 6, the ambiguity in the value of q and its effect on R is small compared to the calculated value of R given below. The basic assumption in the calculation is that the projectiles retain their initial directions of motion while penetrating the target. This assumption is best for the 720 MeV cluster and improves with increasing cluster energy.

In Fig. 7(b) is plotted the stopping ratio as a function of penetration depth for the 720 MeV C_{60} cluster. The stopping ratio is plotted as a function of penetration depth beginning with 40 nm; q in these calculations was assumed to be the ionic charge. From the above discussion the stopping ratio lies between the value given in Fig. 7(b) and 25/36 of this number. Thus the Arista model [7] predicts a significant stopping ratio up to a penetration distance of 90 nm. As the cluster expands with increasing penetration the characteristic linear dimension of the cluster becomes larger with respect to v/ω_p, the domain of the interference effects, thereby causing a decrease in the vicinage effect.

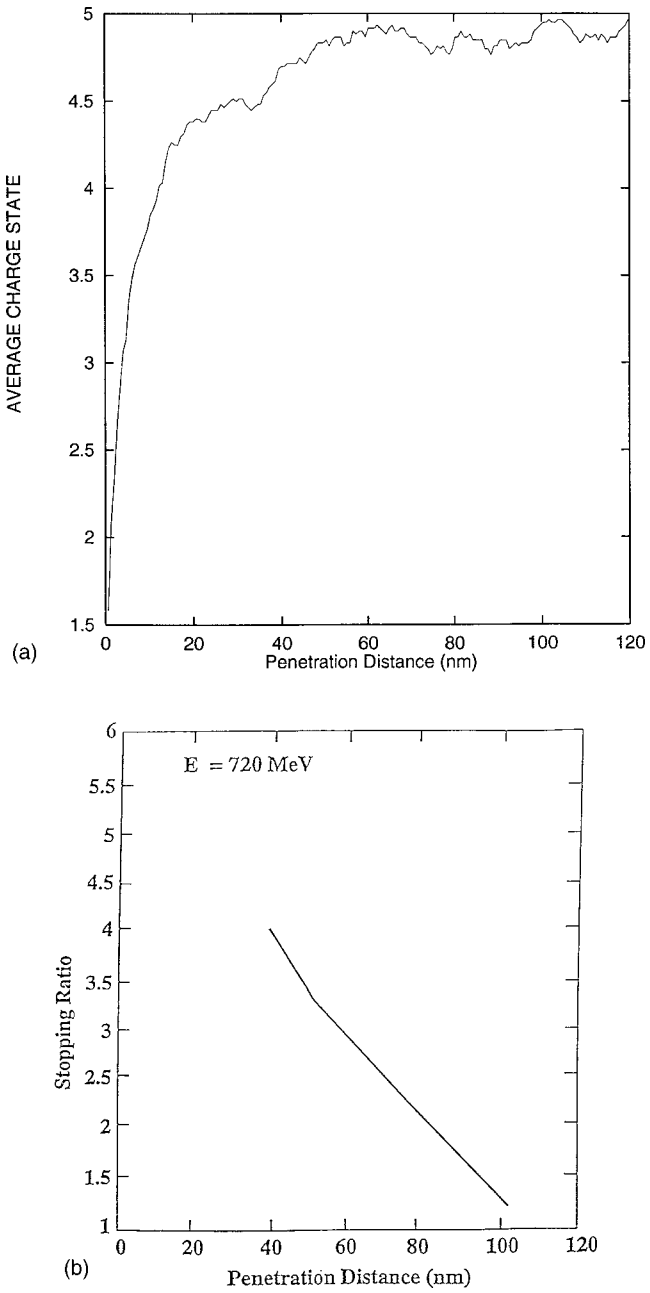

FIG. 7. (a) Average charge state of a 720 MeV cluster as a function of penetration depth. (b) Ratio of the total cluster stopping power divided by the sum of the stopping power of 60 individual carbon ions of the same charge state (stopping ratio), for a total cluster energy of 720 MeV. The stopping ratio is displayed only beyond the point where the charge state is close to 5.

IV. CONCLUSIONS

This paper describes a detailed simulation of the interaction and disruption of a C_{60} cluster penetrating an amorphous target of carbon. In the present calculations multiple scattering and Coulomb explosion as well as the calculation of the charge state are all treated simultaneously. The cluster constituent charge states were obtained by means of Monte Carlo simulation, based on a model proposed by Bell [10], while the multiple scattering using the method of Moller *et al.* [15] was also computed by Monte Carlo simulation. The Coulomb explosion of the cluster was calculated by means of molecular dynamics [21]. Both multiple scattering and Coulomb explosion were computed within the same time step. The algorithm just described permitted the calculation of the effect of the neighboring cluster constituents on the charge state of a given cluster component. At the present stage only the effect on the ionization cross section, which decreases due to the increase in binding energy, was studied. It is noted here that charge-state suppression due to the vicinage effect was calculated by Miskovic *et al.* [30] for small carbon clusters, making use of the Brandt-Kitagawa variational theory [31].

Multiple scattering is the dominant process in the disrup-

tion of the cluster at a total cluster energy of 40 MeV. With an increase in cluster energy, Coulomb explosion becomes the more prominent process, such that at a total cluster energy of 720 MeV it is by far the major disruption mechanism. At a total cluster energy of 144 MeV multiple scattering and Coulomb repulsion make similar contributions to cluster disruption. Statistical aspects of cluster expansion were investigated for the above mentioned three cluster energies. At 40 MeV cluster energy the half-width of the cluster radial distribution divided by the average radius is of the order of 20–25 %.

The spatial correlations between the cluster components are of crucial importance in connection with the process of track formation. This process was studied employing criteria proposed by Tombrello *et al.* [6], which were based on experimental observation. The major feature describing the track radius as a function of penetration depth for a 30 MeV C_{60} cluster incident on a silicon target was thus reproduced. Track splitting observed by Dunlop *et al.* for 40 MeV C_{60} on YIG [2] was also simulated here for an amorphous carbon target provided the interaction was screened by four valence electrons.

Significant enhancement of the energy deposition due to collective (vicinage) effects was calculated for the expanding cluster penetrating the target. This topic was addressed for the cluster energy of 720 MeV, where the ambiguity in defining the charge state has little effect compared to the calculated enhancement in the energy deposition. Generating C_{60} clusters at this energy, however, is beyond the scope of present experimental technique.

Future work on this topic will include the effect of the wake forces on the cluster disruption, similar to Refs. [19] and [24]. The effect of the neighboring cluster constituents on the recombination cross section will also be studied. Thus a fuller description of cluster breakup and of charge-state suppression should be obtained.

Another topic of interest is the experimental and theoretical study of cluster penetration under channeling conditions where the effect of scattering by the target is much reduced. A good example of such a calculation is C_{60} bombarding a quartz crystal in the [001] direction. The crystal channel in this case is large enough to contain the C_{60} cluster. In such a calculation cluster shapes similar to those predicted by Wang *et al.* [26] could perhaps be observed. It should be noted, however, that the density of the electron gas through which the cluster penetrates is appreciably less than for nonchanneling conditions.

Finally, it is suggested here to study track production and especially track splitting in materials with a lower track registration threshold, such as mica. An increase in track splitting should occur in such cases, which could perhaps be successfully simulated. A comparison of track registration and splitting in materials with varying dielectric properties is of special interest in connection with the effect of Coulomb shielding on these processes.

ACKNOWLEDGMENT

The authors are very grateful to Professor P. Sigmund for very stimulating discussions and for many helpful comments.

[1] H. Dammak, A. Dunlop, D. Lesueur, A. Brunelle, and S. Della-Negra, Phys. Rev. Lett. **74**, 1135 (1995).
[2] A. Dunlop, G. Jaskierowicz, J. Jensen, and S. Della-Negra, Nucl. Instrum. Methods Phys. Res. B **132**, 93 (1997).
[3] S. M. M. Ramos, N. Bonardi, B. Canut, S. Bouffard, and S. Della-Negra, Nucl. Instrum. Methods Phys. Res. B **143**, 319 (1998).
[4] A. Brunelle, S. Della-Negra, J. Depauw, D. Jacquet, Y. Le Beyec, M. Pautrat, and Ch. Schoppmann, Nucl. Instrum. Methods Phys. Res. B **125**, 207 (1997).
[5] A. Brunelle, S. Della-Negra, J. Depauw, D. Jacquet, Y. Le Beyec, and M. Pautrat, Phys. Rev. A **59**, 4456 (1999).
[6] T. A. Tombrello, A. M. Childs, and J. W. Hartman, Nucl. Instrum. Methods Phys. Res. B **145**, 429 (1998).
[7] N. R. Arista, Phys. Rev. B **18**, 1 (1978).
[8] J. W. Hartman, T. A. Tombrello, S. Bouneau, S. Della-Negra, D. Jacquet, Y. Le Beyec, and M. Pautrat, Phys. Rev. A **62**, 043202 (2000).
[9] P. Sigmund, I. S. Bitensky, and J. Jensen, Nucl. Instrum. Methods Phys. Res. B **112**, 1 (1996).
[10] G. I. Bell, Phys. Rev. **90**, 548 (1953).
[11] Z. Zinamon, E. Nardi, and M. Hass, Nucl. Instrum. Methods Phys. Res. B **69**, 127 (1992).
[12] E. Nardi and Z. Zinamon, Phys. Rev. A **51**, R3407 (1995).
[13] P. Richard, in *Atomic Inner Shell Processes I*, edited by B. Crassman (Academic, New York, 1975), p. 73.
[14] G. Basbas, W. Brandt, and R. Laubert, Phys. Rev. A **7**, 983 (1973).
[15] W. Moller, G. Popiech, and G. Schrieder, Nucl. Instrum. Methods **130**, 265 (1975).
[16] J. Lindhard, V. Nielson, and M. Scharff, K. Dan. Vidensk. Selsk. Mat. Fys. Medd. **36**, 10 (1968).
[17] L. Meyer, Phys. Status Solidi B **44**, 253 (1971).
[18] D. Zajfman, G. Both, E. P. Kanter, and Z. Vager, Phys. Rev. A **41**, 2482 (1990).
[19] Z. Vager and D. S. Gemmell, Phys. Rev. Lett. **37**, 1352 (1976).
[20] N. Bohr, K. Dan. Vidensk. Selsk. Mat. Fys. Medd. **18**, 8 (1948).
[21] N. Anastasiou and D. Fincham, Comput. Phys. Commun. **25**, 159 (1982).
[22] J. F. Ziegler, J. P. Biersack, and U. Littmark, *Stopping Power and Ranges of Ions in Matter* (Pergamon, New York, 1985), Vol. I.
[23] J. Lindhard, K. Dan. Vidensk. Selsk. Mat. Fys. Medd. **28**, 8 (1954).
[24] I. Abril, R. Garcia-Molina, C. D. Denton, F. J. Perez-Perez, and N. R. Arista, Phys. Rev. A **58**, 357 (1998).
[25] N. D. Mermin, Phys. Rev. B **1**, 2362 (1970).

[26] Y. N. Wang, H. T. Qui, and Z. L. Miskovic, Phys. Rev. Lett. **85**, 1448 (2000).
[27] A. Dunlop, G. Jaskierowicz, and S. Della-Negra, Nucl. Instrum. Methods Phys. Res. B **146**, 302 (1998).
[28] B. Canut, N. Bonardi, S. M. M. Ramos, and S. Della-Negra, Nucl. Instrum. Methods Phys. Res. B **146**, 296 (1998).
[29] J. Jensen and P. Sigmund, Phys. Rev. A **61**, 032903 (2000).
[30] Z. L. Miskovic, S. G. Davison, F. O. Goodman, W.-K. Liu, and Y.-N. Wang, Phys. Rev. A **61**, 062901 (2000).
[31] W. Brandt and M. Kitagawa, Phys. Rev. B **25**, 5631 (1982).